Earthquake Engineering & Structural Dynamics
The Journal of the International Association for Earthquake Engineering

EARTHQUAKE ENGINEERING & STRUCTURAL DYNAMICS
*Earthquake Engng Struct. Dyn.* 2016; **45**:1473–1494
Published online 3 March 2016 in Wiley Online Library (wileyonlinelibrary.com). DOI: 10.1002/eqe.2718

# Development of deformable connection for earthquake-resistant buildings to reduce floor accelerations and force responses

Georgios Tsampras[1,*,†], Richard Sause[1], Dichuan Zhang[2], Robert B. Fleischman[3], Jose I. Restrepo[4], David Mar[5] and Joseph Maffei[6]

[1]*ATLSS Engineering Research Center, Department of Civil and Environmental Engineering, Lehigh University, Bethlehem, PA, USA*
[2]*Department of Civil Engineering, Nazarbayev University, Astana, Kazakhstan*
[3]*Department of Civil Engineering and Engineering Mechanics, University of Arizona, Tucson, AZ, USA*
[4]*Department of Structural Engineering, University of California, San Diego, CA, USA*
[5]*Mar Structural Design, Berkeley, CA, USA*
[6]*Maffei Structural Engineering, Oakland, CA, USA*

## SUMMARY

This paper presents the development of a deformable connection that is used to connect each floor system of the flexible gravity load resisting system (GLRS) with the stiff lateral force resisting system (LFRS) of an earthquake-resistant building. It is shown that the deformable connection acts as a seismic response modification device, which limits the lateral forces transferred from each floor to the LFRS and allows relative motion between the GLRS and LFRS. In addition, the floor accelerations and the LFRS story shears related to the higher-mode responses are reduced. The dispersion of peak responses is also significantly reduced. Numerical simulations of the earthquake response of a 12-story reinforced concrete shear wall example building with deformable connections are used to define an approximate feasible design space for the deformable connection. The responses of the example building model with deformable connections and the example building model with rigid-elastic connections are compared. Two configurations of the deformable connection are studied. In one configuration, a buckling restrained brace is used as the limited-strength load-carrying hysteretic component of the deformable connection, and in the other configuration, a friction device is used. Low damping laminated rubber bearings are used in both configurations to ensure the out-of-plane stability of the LFRS and to provide post-elastic stiffness to the deformable connection. Important experimental results from full-scale tests of the deformable connections are presented and used to calibrate numerical models of the connections. Copyright © 2016 John Wiley & Sons, Ltd.

Received 14 July 2015; Revised 11 January 2016; Accepted 25 January 2016

KEY WORDS: deformable connection; floor accelerations; higher-mode responses; buckling restrained brace; low damping laminated rubber bearings; friction device

## 1. INTRODUCTION

In a conventional earthquake-resistant building system, the gravity load resisting system (GLRS) includes the floor system, where most of the seismic mass is located, and the floor system is rigidly attached to the lateral force resisting system (LFRS), which resists the seismic inertial forces generated by the acceleration of the seismic mass.

It has been shown that the seismic inertial forces generated in the floor system can be large relative to the floor diaphragm strength, and can lead to inelastic and potentially non-ductile

*Correspondence to: Georgios Tsampras, P.C. Rossin Doctoral Fellow, ATLSS Engineering Research Center, Department of Civil and Environmental Engineering, Lehigh University, Bethlehem, PA 18015, USA.
†E-mail: tsampras.g@gmail.com

Copyright © 2016 John Wiley & Sons, Ltd.

response of the diaphragm [1]. The development of excessive inertial forces due to high floor accelerations can produce nonlinear response and serious damage of the LFRS, which may lead to unsatisfactory seismic response [2, 3]. The nonlinear response of the LFRS can act as a 'cut-off' mechanism that may limit the floor accelerations [4–6]. However, even when ductile nonlinear response of the LFRS occurs, high floor accelerations may be observed, due to the response of second and higher modes [5–7]. Studies of LFRS with a predominantly flexural response (e.g. a reinforced concrete cantilever structural wall), which is dominated by nonlinear moment-rotation response at the base of the LFRS, show that high floor accelerations due to the second-mode and higher-mode response can be expected [8–12].

Skinner *et al.* (1975) sketched a building system with a separated tower and a moment-resisting frame connected by hysteretic dampers [13]. This concept allows relative motion between the tower and the frame, and this relative motion enables the hysteretic dampers to dissipate seismic energy [13]. Key (1984) performed a numerical study to assess the effect of using hysteretic dampers to link a stiff structure (shear wall) with a flexible structure (moment-resisting frame) to dissipate energy and improve the structural response [14]. Luco and De Barros (1998) studied the seismic response of a tall building modeled by two shear beams interconnected with stiff or flexible link elements [15].

Mar and Tipping (2000) presented structural details for a story isolation system that reduces the base shear and roof acceleration demands [16]. Amaris *et al.* (2008) and Johnston *et al.* (2014) presented alternative discrete and dissipative connections between the LFRS and floor diaphragm of precast concrete building structures [17, 18]. Buckling restrained braces (BRBs) have been used to connect two buildings to prevent pounding [19].

Crane (2004) conducted shake table tests on two small-scale six-story buildings with energy dissipative connections between the floors and the LFRS [20]. Triangular-plate added damping and stiffness devices were used as the connections. Reduced floor accelerations and base overturning moment were observed [20]. Based on this previous research, studies have been initiated on an earthquake-resistant building system that allows relative motion between the LFRS and GLRS, with goal of reducing the demands in the floor system and LFRS under seismic loading [21–24].

This paper focuses on the development of a deformable connection that limits the lateral forces transferred from each floor of the GLRS to the LFRS. The use of these deformable connections reduces the floor accelerations and the LFRS story shears due to the higher-mode responses, and reduces the dispersion of peak responses. Energy dissipation is provided by the nonlinear hysteretic response of these deformable connections, but is not the main purpose of using them.

In this paper, an initial parametric numerical study identifies the approximate feasible design space for the deformable connection. Two configurations of the deformable connection are presented that could be used with various types of LFRS. Both configurations of the deformable connection are constructable, accessible for inspection, repairable, and provide lateral stability to the flexible GLRS. The expected force-deformation responses of the deformable connections are modeled, and preliminary numerical simulations of a building model with deformable connections show the reduction of the responses at specific floors compared with a conventional building system with rigid-elastic connections. Finally, the force-deformation responses of the deformable connection models are refined based on results from full-scale experiments, and additional numerical simulations are presented. Statistical results of peak responses are presented.

## 2. DEVELOPMENT OF DEFORMABLE CONNECTION

### *2.1. Conceptual design*

Figure 1(a) shows the plan view of a building structural system with the deformable connections in the undeformed condition. Figure 1(b) shows the elevation of the building system in a deformed condition. As seen in Figure 1(a), openings in the floor system are required to allow the relative motion between the LFRS and the floor system. The floor system is connected to the LFRS using a deformable connection that consists of two types of components. The limited-strength hysteretic component is

Copyright © 2016 John Wiley & Sons, Ltd.

DOI: 10.1002/eqe

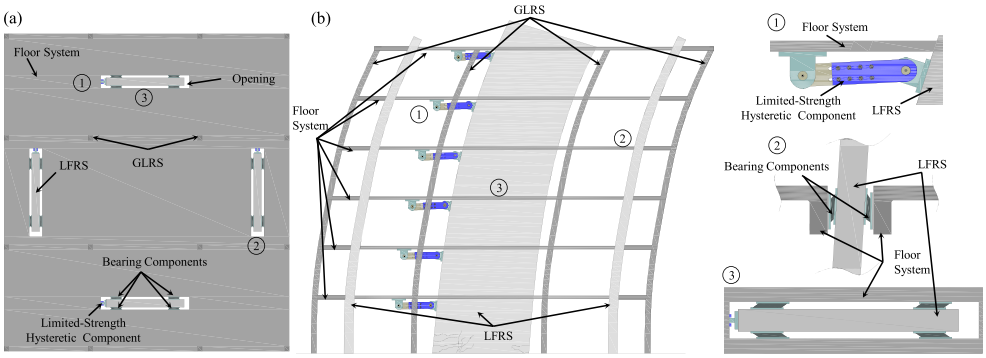



Figure 1. Sketches of earthquake-resistant building system with deformable connections. LFRS, lateral force resisting system; GLRS, gravity load resisting system.

required to transfer lateral forces in the plane of the LFRS from the floor system to the LFRS, and to provide stability to the flexible GLRS. The limited-strength hysteretic component will extend and retract because of the relative horizontal motion in the plane of the LFRS. The bearing components brace the LFRS in the out-of-plane direction. The bearing components must have high compressive stiffness and strength to transfer LFRS out-of-plane bracing forces without significant compressive deformation. To permit relative in-plane motion between the LFRS and the floor system, the bearing components should have low shear stiffness compared with their compressive stiffness. This shear stiffness provides post-elastic stiffness to the deformable connection in the in-plane direction. The close up views of the limited-strength hysteretic and bearing components in Figure 1(b) show the kinematic requirements for the deformable connection based on the expected seismic response of the building. These kinematic requirements are in-plane relative vertical and horizontal motions, and out-of-plane rotation of the LFRS relative to the floor system.

### *2.2. Initial parametric numerical study*

An initial parametric numerical study was conducted to identify the approximate feasible design space for the deformable connection parameters, and to assess the effects of the strength and stiffness of the deformable connection on the seismic response of an example building structure.

*2.2.1. Baseline numerical model of example building with idealized deformable connection.* The example building structure is a 12-story bearing wall system with special reinforced concrete shear walls ($R=5$, $\Omega_o=2.5$, $C_d=5$) [25]. The building plan dimensions are $30.5\times55.0$ m. The ASCE 7–10 design spectrum parameters that were used are $S_1=0.6$ g, $S_s=1.5$ g, $F_a=1.0$, $F_v=1.5$, $T_{long}=8.0$ s, Site Class D, and importance factor $I_e=1.0$ [22]. The first story height is 4.9 m, and the remaining story heights are 3.2 m. The dimensions of the shear walls are $12.8\times0.5$ m. The wall design moment is 290 MNm. The dimensions of the gravity columns over the first seven stories are $0.8\times0.8$ m, and the remaining columns are $0.6\times0.6$ m. Flat slabs are used. The effective width of the slab at each column line is 2.5 m, and the thickness is 0.2 m. The cracked section moment of inertia of the wall, the gravity columns, and the equivalent flat slab beam are assumed to be 35%, 70%, and 25% of the gross section moment of inertia. Half of the structure shown in Figure 2(a), including one shear wall and the GLRS within its seismic tributary area, was used to develop a baseline numerical model in OpenSEES [26] as shown in Figure 2(b). Diaphragm flexibility is not included in the model. The seismic mass associated with the shear wall is 747 kN/g for the first floor and 490 kN/g for the remaining upper floors. The seismic mass associated with each half floor of the GLRS is 5905 kN/g. Elastic beam-column elements were used to model the stiffness of the LFRS (shear wall) and GLRS. Nonlinear flexural response and shear failure were not included in these elements. The GLRS was modeled as a linear elastic moment frame with rigid (not pinned) connections. Geometric nonlinearities were considered. The nonlinear flexural response of the wall was modeled with a nonlinear spring at the base of the wall. An idealized elastic–plastic force-deformation response with kinematic hardening was used to model the deformable connection at each floor as shown in

Copyright © 2016 John Wiley & Sons, Ltd.

DOI: 10.1002/eqe

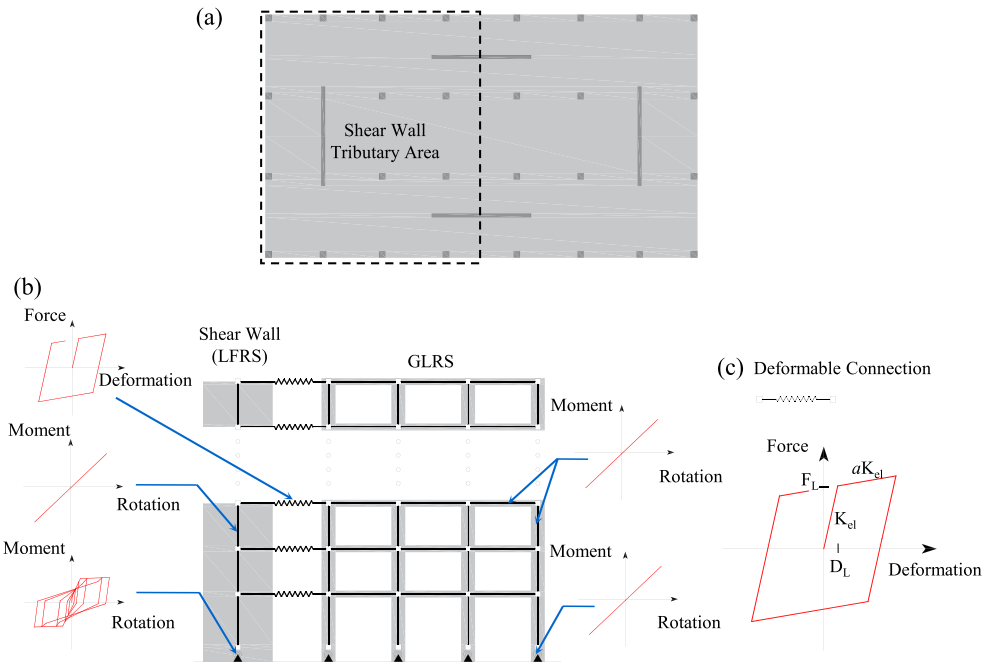



Figure 2. (a) Twelve-story building structure. (b) Model of half of the structure. (c) Idealized deformable connection response. LFRS, lateral force resisting system; GLRS, gravity load resisting system.

Figure 2(c). Rayleigh damping with a 2% damping ratio in modes 1 and 3 was assigned to the elastic beam-column elements of the LFRS and GLRS. No damping was assigned to the wall base nonlinear spring or to the elements that represent the deformable connections.

The deformable connection parameters that were studied are the limiting strength $F_L$ that initiates the transition from the elastic to the post-elastic force-deformation response, the elastic stiffness $K_{el}$, and the post-elastic stiffness $\alpha K_{el}$. The parameters of the deformable connection are the same at each floor (for all the numerical simulations presented in this paper). $F_L$ was normalized by the half 12th floor diaphragm design force, $F_{px}/2 = 1580$ kN, calculated based on ASCE7–10 [22–25]. $K_{el}$ was normalized by a reference stiffness, $K_{ref} = 4.34$ MN/mm. The values assigned to the normalized parameters are $r_f = 2F_L/F_{px} = \{0.1, 0.2, 0.3, 0.4, 0.5, 0.6, 0.7, 0.8, 0.9, 1\}$, $r_k = K_{el}/K_{ref} = \{0.01, 0.03, 0.05, 0.1, 0.3, 0.5, 1.0\}$, and $\alpha = \alpha K_{el}/K_{el} = \{0.0, 0.01, 0.02, 0.03, 0.04, 0.05\}$. Four hundred and twenty different combinations of parameters were used in the parameter study. A system with rigid-elastic (RE) connections ($r_f = 1000$, $r_k = 1000$) was used to represent a conventional system without significant diaphragm flexibility.

*2.2.2. Input ground motions.* Eighteen ground motions were selected from the FEMA P-695 [27] far field set and used as input excitation in the numerical earthquake simulations. Table I gives details of the ground motions. The average method [28] was used to scale the recorded ground motions to match their spectral accelerations to the ASCE7-10 [25] design basis earthquake spectrum over a range of periods T∈ [0.6, 2.0] seconds (Figure 18(b)). All the numerical simulations in this paper use design basis earthquake level ground motions.

*2.2.3. Results.* Figure 3(a) shows the 420 combinations of parameters. For each combination of parameters, Figure 4(a)–(d) shows the mean maximum peak value of the connection deformation $D_c$, the mean maximum peak value of the GLRS story drift $\theta_{GLRS}$, the mean maximum peak value of the floor total acceleration $a_f$, and the mean maximum peak value of the LFRS story shear $V_{LFRS}$, respectively, where 'peak' refers to the maximum absolute value from the time history response at each floor (or story), 'maximum' refers to the maximum peak over all floors (or stories), and 'mean' refers to the mean maximum peak value for the set of ground motions. In the figures, the variation of $r_f$ is represented on the $x$-axis, the variation of $r_k$ is represented with different colors, and the

Copyright © 2016 John Wiley & Sons, Ltd.

DOI: 10.1002/eqe

Table I. Eighteen ground motions selected from 44 FEMA P-695 far-field earthquake ground motion set.

| EQ# | Event | M | Year | Distance [km] | Soil type class | Component | [a]PGA [g] | [a]PGV [cm/s] | [b]SF |
|---|---|---|---|---|---|---|---|---|---|
| 1 | Friuli Italy | 6.5 | 1976 | 15.0 | C | TMZ000 | 0.35 | 22 | 2.77 |
| 2 | Duzce Turkey | 7.1 | 1999 | 12.0 | D | BOL000 | 0.73 | 56 | 0.99 |
| 3 | Superstition Hills | 6.5 | 1978 | 11.2 | D | B-POE270 | 0.45 | 36 | 1.87 |
| 4 | Superstition Hills | 6.5 | 1978 | 11.2 | D | B-POE360 | 0.30 | 33 | 1.97 |
| 5 | Chi-Chi Taiwan | 7.6 | 1999 | 10.0 | D | E – W | 0.35 | 71 | 1.33 |
| 6 | Chi-Chi Taiwan | 7.6 | 1999 | 10.0 | D | N – S | 0.44 | 115 | 0.84 |
| 7 | Landers | 7.3 | 1992 | 19.7 | D | CLW-LN | 0.28 | 26 | 2.54 |
| 8 | Imperial Valley | 6.5 | 1979 | 22.0 | D | H-DLT262 | 0.24 | 26 | 1.90 |
| 9 | Imperial Valley | 6.5 | 1979 | 22.0 | D | H-DLT352 | 0.35 | 33 | 1.28 |
| 10 | Imperial Valley | 6.5 | 1979 | 12.5 | D | H-E11230 | 0.38 | 42 | 2.06 |
| 11 | Northridge | 6.7 | 1994 | 9.4 | D | MUL279 | 0.52 | 63 | 0.71 |
| 12 | Superstition Hills | 6.5 | 1978 | 18.2 | D | ICC000 | 0.36 | 46 | 1.42 |
| 13 | Loma Prieta | 6.9 | 1989 | 12.2 | D | G03090 | 0.37 | 45 | 1.40 |
| 14 | Kocaeli Turkey | 7.5 | 1999 | 13.6 | D | DZC180 | 0.31 | 59 | 1.53 |
| 15 | Kocaeli Turkey | 7.5 | 1999 | 13.6 | D | DZC270 | 0.36 | 46 | 0.93 |
| 16 | Cape Mendocino | 7.0 | 1992 | 7.9 | D | RIO270 | 0.39 | 44 | 1.27 |
| 17 | Kobe Japan | 6.9 | 1995 | 19.1 | D | SHI090 | 0.21 | 28 | 1.66 |
| 18 | Landers | 7.3 | 1992 | 23.6 | D | YER270 | 0.24 | 51 | 1.24 |

[a]For original earthquake ground motion records
[b]Scale factor (SF) to match design spectral accelerations over period range T∈[0.6, 2.0] seconds

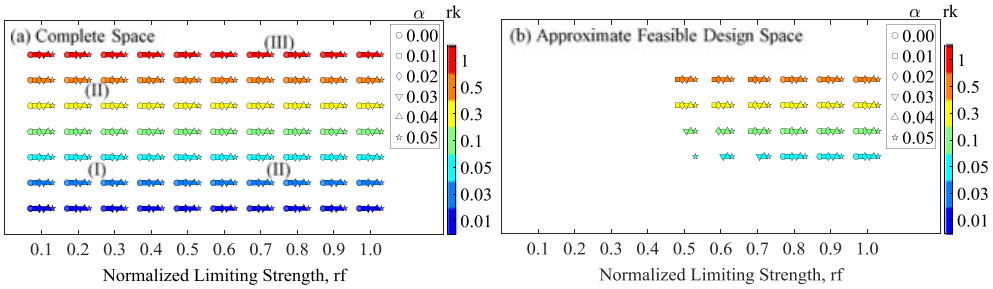



Figure 3. (a) Complete parameter space. (b) Approximate feasible design space.

variation of $a$ is represented with different symbols. The response of the system with RE connections is represented with a solid black circle.

Figure 4(a) shows that as $r_f$ and $r_k$ decrease, the mean maximum peak $D_c$ increases. An approximate upper limit on the mean maximum peak $D_c$ of 100 mm was assumed as the maximum feasible connection deformation for the design earthquake, as shown in Figure 4(a) with a dashed line. A deformation capacity greater than this value is needed to accommodate the maximum considered earthquake demands. Figure 3(b) shows the approximate feasible design space for the deformable connection parameters, which defines the feasible range of values for (i) the limiting strength of the connections, $F_L$, (ii) the elastic stiffness of the connection, $K_{el}$, (iii) the post-elastic stiffness of the connection, $\alpha$.

Many combinations of parameters have been excluded from the approximate feasible design space because the mean maximum peak $D_c$ exceeds 100 mm (approximate region I in Figure 3(a)), or because the combination of $F_L$ and $K_{el}$ is expected to be difficult to achieve in a practical design (approximate regions II in Figure 3(a)), or because $K_{el}$ is too high to achieve in a practical design (approximate region III in Figure 3(a)).

Figure 4(b) shows that systems with a combination of parameters within the approximate feasible design space have a mean maximum peak $\theta_{GLRS}$ that varies from 1.0% to 1.5% rad. The mean maximum peak $a_f$ and mean maximum peak $V_{LFRS}$ of the system with deformable connections are reduced relative to the system with RE connections as shown in Figure 4(c) and (d), respectively.

Copyright © 2016 John Wiley & Sons, Ltd.

DOI: 10.1002/eqe

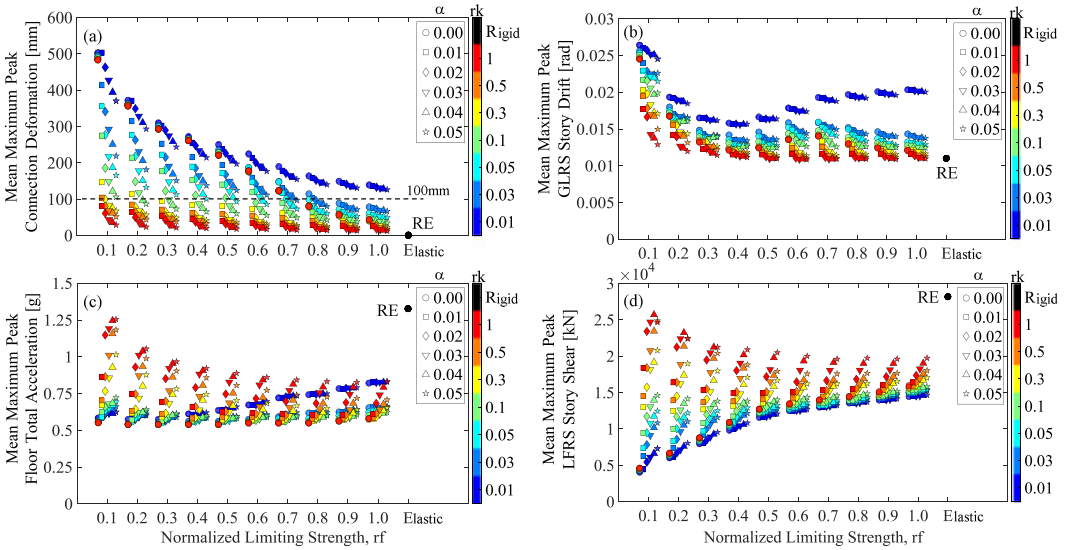



Figure 4. Mean maximum peak (a) connection deformation, (b) gravity load resisting system (GLRS) story drift, (c) floor total acceleration, and (d) lateral force resisting system (LFRS) story shear from initial parametric numerical study. RE, rigid elastic.

Table II. Response for design cases 1 and 2 and system with RE connections.

| | | | | Mean maximum peak values | | | |
|---|---|---|---|---|---|---|---|
| | $r_f$ [−] | $r_k$ [−] | $\alpha$ [−] | $D_c$ [mm] | $\theta_{GLRS}$ [rad] | $a_f$ [g] | $V_{LFRS}$ [kN] |
| RE | 1000 | 1000 | 0.00 | 0 | 0.0110 | 1.33 | 28156 |
| Design case 1 | 0.6 | 0.05 | 0.03 | 107 | 0.0140 | 0.59 | 13200 |
| Design case 2 | 1.0 | 0.10 | 0.03 | 38 | 0.0125 | 0.61 | 15550 |

RE, rigid elastic.

Two different design cases that represent deformable connections with significantly different limiting strengths are used to illustrate these response reductions as follows. The parameters for design case 1 are $r_f = 0.6$, $r_k = 0.05$, and $a = 0.03$, and the parameters for design case 2 are $r_f = 1.0$, $r_k = 0.1$, and $\alpha = 0.03$. Table II shows that for both design cases, the mean maximum peak $a_f$ and mean maximum peak $V_{LFRS}$ are approximately half of those for the system with RE connections. The mean maximum peak $\theta_{GLRS}$ increases relative to the system with RE connections by 27% and 14% for design case 1 and 2, respectively. The mean maximum peak $D_c$ was significantly smaller for design case 2.

### *2.3. Follow-up parametric numerical study*

A follow-up parametric numerical study was used to assess the effect of the base hinge strength of the shear wall, and the LFRS and GLRS stiffness in the numerical model of the example building on the mean maximum peak $a_f$, $\theta_{GLRS}$, and $V_{LFRS}$. The baseline numerical model was used along with the deformable connection parameters from design cases 1 and 2. Three additional models were studied. For each model, either the base hinge moment capacity, the moment of inertia of the gravity columns, or the moment of inertia of the shear wall was reduced by 50% compared with the baseline model. Figure 5 shows the mean maximum peak response quantities, normalized by the mean maximum peak response quantities for the baseline model. The normalized mean maximum peak $a_f$ is not affected significantly by changing any of these parameters. The normalized mean maximum peak $V_{LFRS}$ is reduced by reducing the strength of the base hinge. The normalized mean maximum peak $\theta_{GLRS}$ increases when the GLRS flexural stiffness decreases, but the GLRS remains stable.

Copyright © 2016 John Wiley & Sons, Ltd.

DOI: 10.1002/eqe

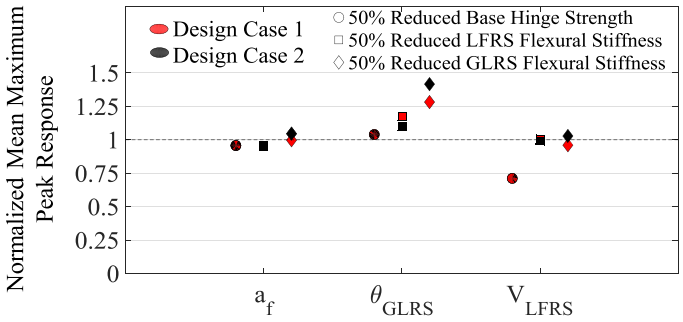



Figure 5. Normalized responses for models with reduced lateral force resisting system (LFRS) or gravity load resisting system (GLRS) parameters.

### 2.4. *Candidate devices for the deformable connection components*

To further develop the deformable connection, various types of existing structural components and devices, which could have the stiffness, strength, and deformation capacity suggested by the approximate feasible design space, were considered.

*2.4.1. Limited-strength hysteretic components. Metallic dampers* (ADAS and TADAS dampers) [29–32] have experimentally validated stable nonlinear hysteretic response and are insensitive to ambient temperature. However, the relatively low yield force and elastic stiffness of ADAS and TADAS dampers compared with the values of $F_L$, and $K_{el}$ within the approximate feasible design space makes these dampers undesirable for this application. In addition, ADAS and TADAS dampers cannot accommodate the kinematic requirements for the deformable connection shown in Figure 1(b).

*Buckling restrained braces* are often used in seismic design practice and are commercially available. Individual BRBs have stable nonlinear hysteretic response [33–35]. The yield force and elastic stiffness of a BRB are closely related, but it is possible to design a BRB to be the limited-strength hysteretic component of a deformable connection with the required $F_L$, $K_{el}$, and deformation capacity. To remain below the axial strain limit for a BRB, a long BRB core (i.e., the yielding zone) is required when the deformation ($D_c$) demand is large. The long core results in a longer and more flexible BRB. Thus, a BRB is more appropriate for deformable connections with a higher $F_L$ and smaller $D_c$ demand within the approximate feasible design space.

*Viscous dampers* are widely used to provide additional damping, remain undamaged under deformation demands within their design limits, and are able to accommodate the kinematic requirements shown in Figure 1. However, a viscous damper cannot serve as the limited-strength hysteretic component because it cannot provide $K_{el}$ to maintain stability of the GLRS under static gravity loads.

*Friction devices* have friction force and elastic stiffness that are not closely related. Thus, a friction device (FD) can provide a wide range of combinations of $F_L$ and $K_{el}$. This characteristic makes FDs excellent candidates for the limited-strength hysteretic component. Prior research [36–41] provides the basis for developing an FD suitable for the deformable connection.

Other potentially useful devices, such as *lead extrusion dampers* [42, 43], *self-centering energy dissipative braces* [44–47], *self-centering buckling restrained braces* [48], *energy dissipating restraints* [49, 50], and *modular buckling restrained braces* [51, 52], were not considered in this study.

*2.4.2. Bearing components. Low damping laminated rubber bearings* (RB) were selected for the bearing components. Each bearing consists of a laminated rubber pad that is bonded to two steel end plates. The laminated rubber pad consists of rubber layers laminated to steel (or carbon fiber) shim plates, which reinforce the rubber for stability. Their compressive stiffness is significantly higher than their shear stiffness. RB have large shear deformation capacity, and their response is approximately linear elastic [53] compared with the expected hysteretic response of the limited-strength hysteretic component.

Copyright © 2016 John Wiley & Sons, Ltd.

DOI: 10.1002/eqe

### *2.5. Proposed configurations of the deformable connection*

Two configurations of the deformable connection are presented in this paper. The first configuration uses a BRB and a set of RB (denoted BRB + RB). The second configuration uses an FD and a set of RB (denoted FD + RB). Comparing the two configurations, the BRB is expected to have smaller elastic stiffness than the FD when used as limited-strength hysteretic components designed for the same $F_L$. In addition, the force-deformation behavior of the BRB is expected to exhibit isotropic hardening and non-zero post-elastic stiffness [35], which are not expected for the FD. Finally, when they designed for the same deformation demand, the length of the BRB will be greater than the length of the FD.

Figure 6 shows sketches of the proposed deformable connections installed in a shear wall building structure. Both the BRB and FD are attached to the LFRS and the floor system using clevis connections. Spherical bearings are used at both ends of the BRB and FD to accommodate the kinematic requirements shown in Figure 1 and ensure the development of only axial forces in the limited-strength hysteretic components. The clevis connections should be capacity-designed for the peak force expected from the limited-strength hysteretic component.

### *2.6. Design concepts*

This section describes design concepts for the deformable connection components, considering the example building structure discussed in Section 2.2.1. Figure 7(a) and (b) shows the components of the BRB and FD.

For design case 1, the BRB + RB connection is designed for a required $F_L = 950$ kN (i.e., $r_f = 0.6$ and $F_L$ is 60% of half 12th floor diaphragm design force $F_{px}/2 = 1580$ kN). The required initial yield force of the BRB is $(1-\alpha)F_L$; however, $\alpha$ is expected to be relatively small (about 5% or less) and is initially unknown, so to simplify the initial design calculations, $\alpha$ is neglected and $F_L$ is taken equal to the BRB initial yield force. Assuming that the yielding zone of the BRB, shown in Figure 7(a), is made from

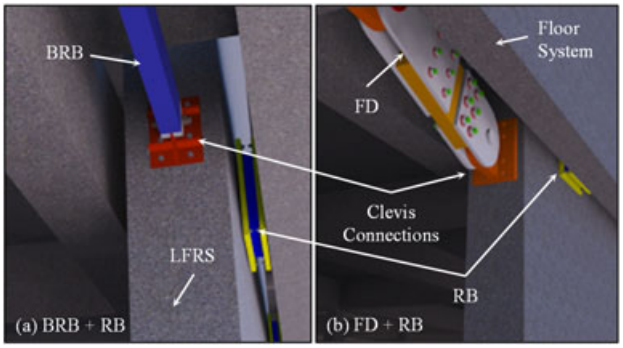



Figure 6. Configurations of deformable connection with (a) buckling restrained brace (BRB) and low damping laminated rubber bearings (RB) and (b) friction device (FD) and low damping laminated rubber bearings. LFRS, lateral force resisting system.

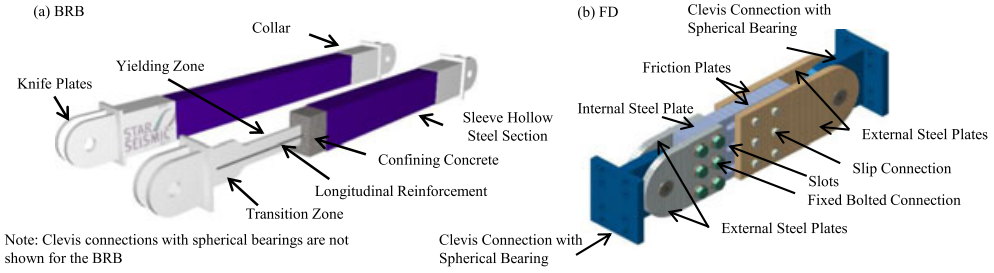



Figure 7. Components of (a) buckling restrained brace (BRB) and (b) friction device (FD).

Copyright © 2016 John Wiley & Sons, Ltd.

DOI: 10.1002/eqe

ASTM A36 steel with actual yielding stress $F_{ya}=280$ MPa, the required yielding zone cross section area is $A_{yz}=F_L/F_{ya}$, which is approximately 3500 mm$^2$. The BRB + RB connection is designed for a required $K_{el}=245$ kN/mm (i.e, $r_k=0.06$, and $K_{el}$ is 6% of the reference stiffness $K_{ref}=4.34$ MN/mm). The required axial elastic stiffness of the BRB is $(1-\alpha)K_{el}$; however, $\alpha$ is neglected initially, and $K_{el}$ is taken equal to the BRB axial elastic stiffness. To account for the flexibility of the clevis connections and other elastic components of the BRB, the axial elastic stiffness of the yielding zone is taken as 1.25 times the axial elastic stiffness of the BRB. The corresponding BRB yielding zone length that provides the required $K_{el}$ is $L_{yz}=2.3$ m. If the axial strain limit for the yielding zone is assumed to be 2.2% (a typical, conservative BRB yielding zone strain limit), the resulting deformation capacity for the yielding zone $D_{byz,c}=50$ mm, which is smaller than the mean maximum peak $D_c=107$ mm expected for design case 1 (Table II). $D_{byz,c}$ can be increased to 107 mm by increasing the yielding zone strain limit to 4.7% or by increasing $L_{yz}$ to 4.9 m (with a 2.2% yielding zone strain limit). However, increasing $L_{yz}$ to 4.9 m will reduce the BRB axial stiffness so that $K_{el}$ would fall below the lower bound of the approximate feasible design space. Therefore, it is not possible to meet the 2.2% strain limit, provide the required $K_{el}$, and provide the required deformation capacity $D_c=107$ mm for design case 1.

For design case 2, the BRB + RB connection is designed for a required $F_L=1580$ kN (i.e., $r_f=1.0$, $F_L$ is 100% of $F_{px}/2=1580$ kN). The required $A_{yz}$ is approximately 5600 mm$^2$. For $L_{yz}=2.3$ m, the BRB axial elastic stiffness is approximately 400 kN/mm (i.e., $r_k=0.1$, $K_{el}$ is approximately 10% of the reference stiffness $K_{ref}=4.34$ MN/mm). At the yielding zone axial strain limit of 2.2%, $D_{byz,c}=50$ mm, which is greater than the mean maximum peak $D_c=38$ mm (Table II). Therefore, it is possible to meet the 2.2% axial strain limit, provide the required $K_{el}$, and provide the required deformation capacity $D_c=38$ mm for design case 2.

The FD + RB connection is designed for a required $F_L$ of 950 kN for design case 1 and 1580 kN for design case 2. The required friction force of the FD is $(1-\alpha)F_L$; however, $\alpha$ is neglected initially, and $F_L$ is taken equal to the FD friction force $F_s$. Coulomb theory is used to estimate $F_s$. A friction interface is created between each friction plate and external steel plate (Figure 7(b)). For two friction interfaces, $n_s=2$, an assumed friction coefficient $\mu=0.35$, and a required $F_s$, the required normal force on the friction interfaces is $N=F_s/\mu n_s$. For design case 1 (i.e., $F_s=F_L=950$ kN), the required $N$ is approximately 1400 kN, and for design case 2 (i.e., $F_s=F_L=1580$ kN), the required $N$ is approximately 2300 kN. Six and 10 ASTM A325 25-mm diameter bolts pre-tensioned to 227 kN are used for design cases 1 and 2, respectively. The FD deformation capacity is a function of the slot length in the internal steel plate. The required deformation capacity $D_c$ of 100 mm can be accommodated using an FD, which is shorter than the corresponding BRB. The FD elastic stiffness will be easily within the approximate feasible design space.

The RB are designed for the connection post-elastic stiffness expressed by the parameter $\alpha$. Based on results from the parametric numerical simulations, the target post-elastic stiffness is assumed to be approximately 8 kN/mm and required RB shear deformation is assumed to be $D_{RB,d}=D_c=100$ mm. The shear strain $\gamma$ limit for elastic response of low damping rubber bearings is between 100% and 200% [54–57]. Assuming a shear strain design limit $\gamma_d=200\%$, the required total thickness of all rubber layers in an RB is $h_{rt}=D_{RB,d}/\gamma_d=50$ mm. The material of the RB is assumed to be 50+/−5 Duro Grade 3 with a shear modulus $G=0.9$ MPa [58]. Table III lists the resulting dimensions of the RB. $W$ and $L$ are the plan dimensions of the rubber pad, $A$ is the area of the rubber pad, $h_{rt}$ is the total thickness of the rubber layers, $n_L$ is the number of layers, $S$ is the shape factor of the rubber layers, $K_{RB}$ is the shear stiffness, $E_c$ is the compressive modulus of the rubber pad, and $K_c$ is the compressive stiffness of the rubber pad. With four RB in the deformable connection, the total shear stiffness $4K_{RB}=8.8$ kN/mm. Shear and compressive strain checks related

Table III. Dimensions and nominal properties of low damping laminated rubber bearings.

| $W$ [mm] | $L$ [mm] | $A=WL$ [mm$^2$] | $h_{rt}$ [mm] | $n_L$ [−] | $h_{ri}=h_{rt}/n_L$ [mm] | $S=A/[2h_{ri}(W+L)]$ [−] | $G$ [MPa] | $K_{RB}=GA/h_{rt}$ [kN/mm] | $E_c=6GS^2$ [MPa] | $K_c=E_cA/h_{rt}$ [kN/mm] |
|---|---|---|---|---|---|---|---|---|---|---|
| 355.6 | 355.6 | 126451 | 50 | 4 | 12.5 | 7 | 0.9 | 2.2 | 263.5 | 655.9 |

Copyright © 2016 John Wiley & Sons, Ltd.

DOI: 10.1002/eqe

to combined compression, rotation and shear due to the kinematic requirements shown in Figure 1 were performed considering the AASHTO specifications [58, 59] and the references [60, 61].

### *2.7. Preliminary study of baseline numerical model with deformable connection models based on expected force-deformation response*

A set of numerical simulations was conducted to provide input for full-scale experiments on the proposed BRB + RB and FD + RB deformable connections. The 18 earthquake input ground motions listed in Table I were used in the simulations. The simulation results provided target seismic deformation histories for the experiments. The experimental force-deformation responses were used to calibrate deformable connection numerical models as described in Section 3.2. This section presents results from two of the 18 ground motions that have quite different spectral pseudo accelerations at short periods.

*2.7.1. Models for preliminary BRB + RB and FD + RB connections.* The baseline model was updated using models of the expected force-deformation response of the BRB + RB connection and the FD + RB connection. The Giuffre–Menegotto–Pinto material model in OpenSEES [26] was used to model the BRB force-deformation response. It was calibrated based on experimental results from Merritt *et al.* [35] as shown in Figure 8(a). An elastic-perfectly plastic model was used for the force-deformation response of the FD as shown in Figure 8(b). A linear elastic model was used for the RB force-deformation response as shown in Figure 8(c). A similar conceptual design was assumed for both the BRB + RB and FD + RB deformable connections. As mentioned earlier, $(1-\alpha)F_L$ is the initial yield force of the BRB and the friction force of the FD. In this preliminary study, $(1-\alpha)F_L$ of the BRB and FD models are 996 kN and 1008 kN, respectively. The axial elastic stiffness $(1-\alpha)K_{el}$ of the BRB and FD models are 356 and 417 kN/mm, respectively. The total RB shear stiffness (which corresponds to $\alpha K_{el}$) is 8.2 kN/mm. Figure 8(d) shows the numerical force-deformation response of the BRB + RB connection and FD + RB connection under cyclic symmetric deformation.

*2.7.2. Ground motions and system dynamic properties.* Figure 9 compares the 5% damping pseudo acceleration response spectra for two of the 18 ground motions (Table I) with the design response spectrum [25]. The spectral pseudo acceleration of the ground motions is close to the design spectral acceleration near the first mode period. However, the TMZ000 (EQ1) ground motion has larger spectral pseudo acceleration than the CHY101 (EQ6) ground motion in the approximate period range of 0.1 to 0.6 s, which includes the second and third mode periods. Figure 9 shows also the lateral displaced shapes of the GLRS for the first three modes (plotted as $\Gamma_n\boldsymbol{\phi}_n$, where $\Gamma_n$, $\boldsymbol{\phi}_n$

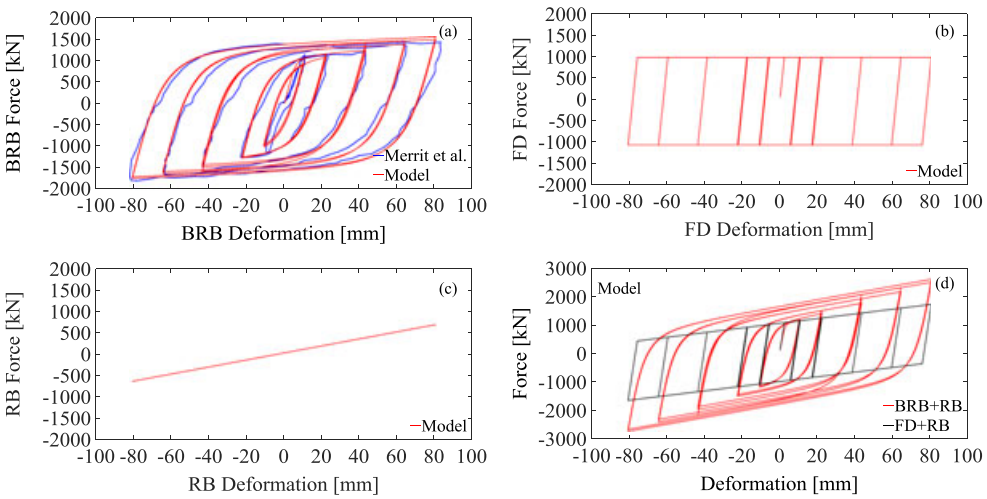



Figure 8. Numerical force-deformation response: (a) buckling restrained brace (BRB) model versus test results (Merritt *et al.*, 2003 [35]), (b) friction device (FD) model, (c) low damping laminated rubber bearings (RB) model and (d) models for two deformable connection configurations.

Copyright © 2016 John Wiley & Sons, Ltd.

DOI: 10.1002/eqe

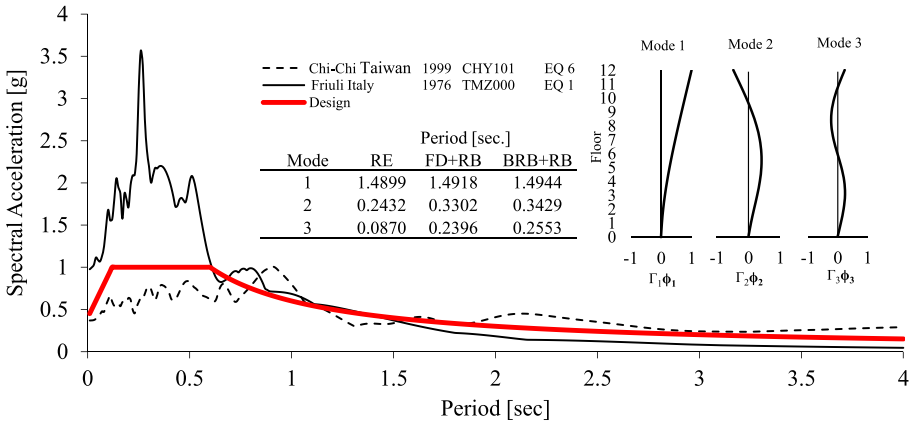



Figure 9. Pseudo acceleration response spectra for 5% damping and first three mode shapes. FD, friction device; RB, low damping laminated rubber bearings; RE, rigid elastic; BRB, buckling restrained brace.

are defined in [8]). The node in the second mode shape is located close to the 10th floor, and the minimum and maximum displacements of the second mode shape are at 6th and 12th floors, respectively.

*2.7.3. Results.* Figure 10(a)–(c) and (d)–(f) shows the 6th, 10th, and 12th floor $a_f$ for EQ1 and EQ6, respectively. The grey line shows the response of the conventional system with RE connections, the black line shows the response of the system with the FD + RB connections, and the red line shows the response of system with the BRB + RB connections. For EQ1, with larger spectral pseudo acceleration in the period range that includes the second and third mode period, $a_f$ for the system with RE connections is large at the 6th and 12th floors. For EQ1, the systems with deformable connections have much smaller $a_f$ at these floors. For EQ6, with smaller spectral pseudo acceleration in the period range of interest, $a_f$ is similar for the system with RE connections and the systems with deformable connections at the 6th and 12th floors, presumably due to the small second mode response at these floors. At the 10th floor, the system with RE connections does not have large values of $a_f$ for either EQ1 or EQ6; $a_f$ is similar for the system with RE connections and the systems with deformable connections. The peak $a_f$ for both EQ1 and EQ6 is similar at all floors for the systems with deformable connections. The deformable connections are quite effective at reducing $a_f$ at floors with large second mode response.

Figure 11 shows the profiles of $V_{LFRS}$ and $\theta_{GLRS}$ at the time of the maximum peak values for EQ1 and EQ6. The maximum peak $V_{LFRS}$ for the system with RE connections is observed at the base of the LFRS and is larger for EQ1 than for EQ6, because of the larger second mode response. The maximum peak $V_{LFRS}$ was reduced significantly by using deformable connections for EQ1. The reduction was less for EQ6. The two systems with deformable connections have similar profiles of $V_{LFRS}$ over the height of the structure at the time of the maximum peak $V_{LFRS}$ for both EQ1 and EQ6.

For EQ1, the maximum peak $\theta_{GLRS}$ for the systems with RE connections or FD + RB connections is 0.012 rad, and for the system with BRB + RB connections is 0.011 rad. For EQ6, the maximum peak $\theta_{GLRS}$ for the systems with RE connections or BRB + RB connections is 0.010 rad and for the system with the FD + RB connections is 0.012 rad.

Thus, the limited forces transferred from the floor systems to the LFRS by the deformable connections reduce the maximum peak $a_f$ and $V_{LFRS}$ without significantly increasing the maximum peak $\theta_{GLRS}$. However, the reduction of response from using deformable connections varies over the height of the structure and with the ground motion.

## 3. EXPERIMENTAL PROGRAM

The BRB + RB connection and FD + RB connection studied in the preliminary numerical simulations were studied experimentally at the NEES@Lehigh Real-Time Multi-Directional (RTMD) earthquake

Copyright © 2016 John Wiley & Sons, Ltd.

DOI: 10.1002/eqe

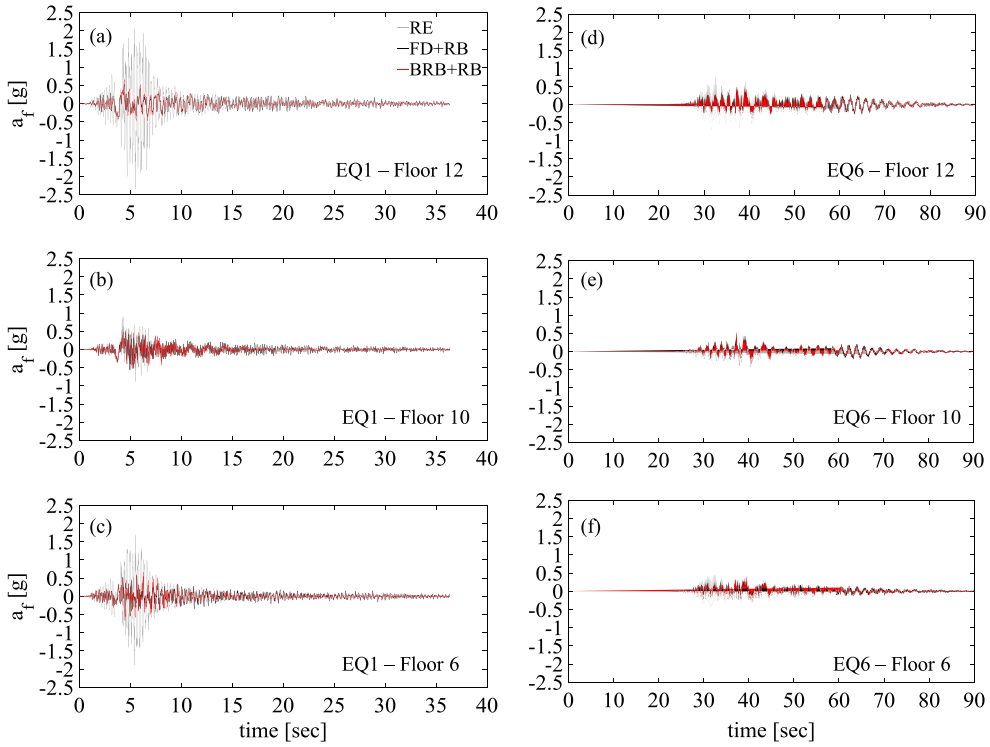



Figure 10. Floor total acceleration response for EQ1 and EQ6. FD, friction device; RB, low damping laminated rubber bearings; RE, rigid elastic; BRB, buckling restrained brace.

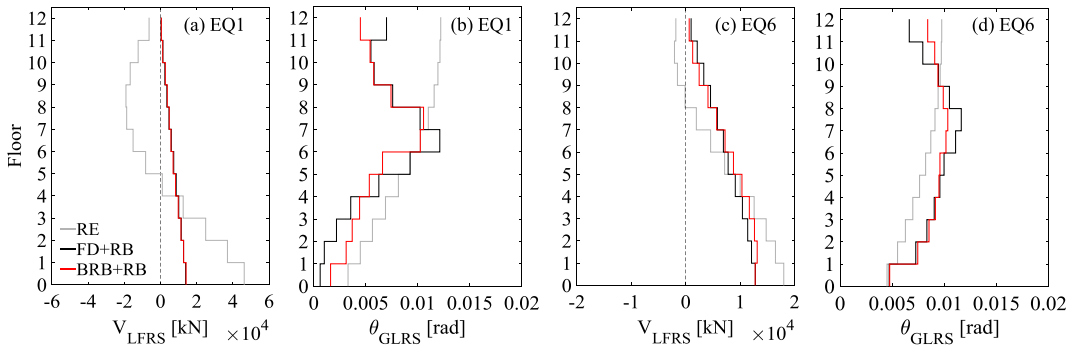



Figure 11. $V_{LFRS}$ and $\theta_{GLRS}$ profiles at time of maximum peak values for EQ1 and EQ6. LFRS, lateral force resisting system; GLRS, gravity load resisting system.

simulation facility at the Advanced Technology for Large Structural Systems (ATLSS) Engineering Research Center [24]. The objectives of the experimental program are (i) to demonstrate the feasibility of designing and constructing the proposed deformable connection configurations for full-scale seismic demands for the 12-story example building structure; (ii) to assess the process for installing the components of the deformable connections; and (iii) to validate the response of the deformable connections under sinusoidal displacement histories and under displacement histories that represent expected seismic deformation demands. The experimental program and the results associated with the force-deformation response of the full-scale components are described in [24]. Here, the experimental setup is presented to demonstrate that the full-scale components of the deformable connections can be installed in a building. A comparison of the two full-scale deformable connection force-deformation responses is presented. The experimental results were used to calibrate numerical models of the BRB + RB connection and the FD + RB connection.

Copyright © 2016 John Wiley & Sons, Ltd.

DOI: 10.1002/eqe

Note that in related research, a half-scale four story rocking precast shear wall building structure with deformable connections was tested at the NEES@UCSD Large High Performance Outdoor Shake Table (LHPOST) [22].

### *3.1. Experimental setup*

The experimental setup includes a portion of the 12-story example building structure. Small parts of the 12th-floor and the reinforced concrete shear wall (LFRS) were built in the laboratory. The components of each deformable connection configuration were attached to these parts of the floor system and wall. Figure 12(a) shows the experimental setup for the BRB + RB connection that includes steel reinforced RB. Figure 12(b) and (c) shows close up views of the BRB and the steel reinforced RB, respectively. Figure 13(a) shows the experimental setup for the FD + RB connection that includes carbon fiber reinforced RB. Figure 13(b) and (c) shows close up views of the FD [24] after and before installation in the experimental setup, respectively. Clevises with spherical bearings were used to attach the BRB and the FD to the LFRS and floor system.

### *3.2. Experimental results and calibration of numerical models*

Figure 14(a) shows the experimental force-deformation responses of the BRB + RB connection and its individual components subjected to the seismic deformation demand shown in Figure 14(b). This

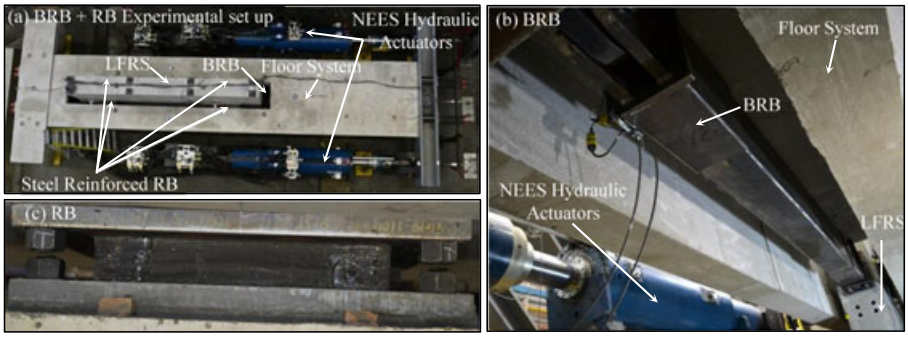



Figure 12. (a) Experimental setup for BRB + RB connection, (b) buckling restrained brace (BRB) and (c) steel reinforced low damping laminated rubber bearings (RB). LFRS, lateral force resisting system; NEES, Network for Earthquake Engineering Simulation.

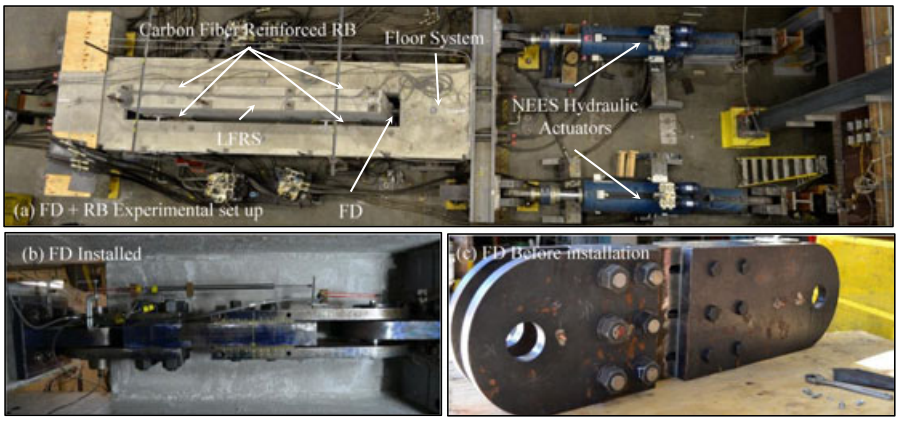



Figure 13. (a) Experimental setup for FD + RB connection, (b) friction device (FD) installed and (c) FD before installation. RB, low damping laminated rubber bearings; LFRS, lateral force resisting system; NEES, Network for Earthquake Engineering Simulation.

Copyright © 2016 John Wiley & Sons, Ltd.

DOI: 10.1002/eqe

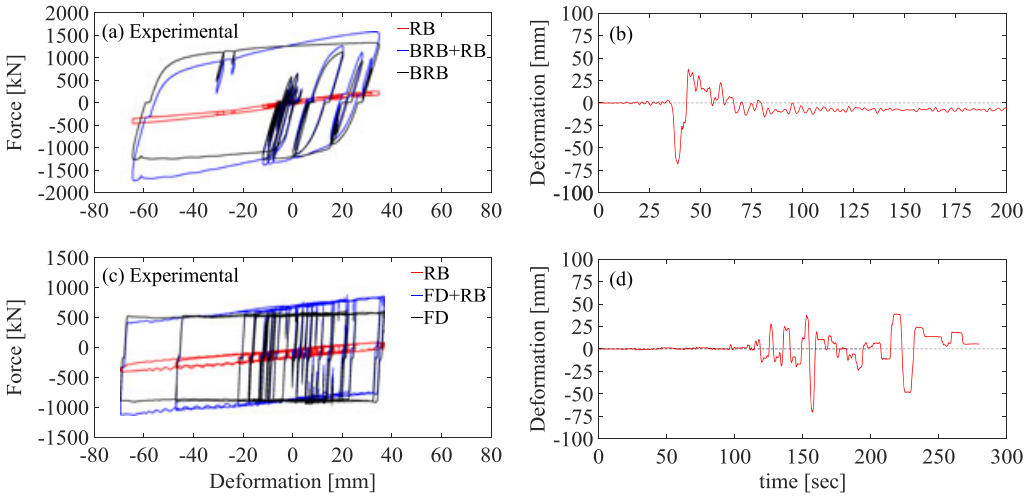



Figure 14. Force-deformation experimental response of deformable connections. RB, low damping laminated rubber bearings; BRB, buckling restrained brace; FD, friction device.

deformation demand is from the 12th-floor response of the example building structure due to EQ1 (Table I). The deformation demand was applied pseudo-statically at a rate 0.1 times the actual EQ deformation rate. The force in the BRB was measured using a load cell (i.e., a pin load cell) in one of the clevises. The force in the steel reinforced RB was estimated indirectly by subtracting the BRB force from the total forces in the actuators. The estimated RB force includes approximately 30 kN of frictional force at the Teflon-steel interface between the floor system and its support columns [24]. The deformable connection hysteretic response was stable under large deformations. The attachments of the deformable connection to the wall and floor behaved as expected. The RB added measurable stiffness to the deformable connections. The gap between the pin and the clevis holes at the BRB ends results in a small deformation offset when the force is approximately zero in the BRB (previously observed in [35]) and BRB + RB force-deformation response.

Figure 14(c) shows the experimental force-deformation responses of the FD + RB connection and its individual components subjected to the seismic deformation demand shown in Figure 14(d). This deformation demand is from the 12th-floor response due to EQ7 (Table I). The deformation demand was applied pseudo-statically at a rate 0.1 times the actual EQ deformation rate. The forces for the FD + RB connection were determined as for the BRB + RB connection. The FD + RB connection hysteretic response was stable under large deformations. The FD response was essentially elastic-perfectly plastic, and the friction force was consistent throughout the test in both extension and retraction of the FD. The RB provided all of the post-elastic stiffness of the FD + RB connection.

For the BRB + RB and FD + RB connections, the experimentally observed $K_{el}$ was 190 kN/mm and 1730 kN/mm (i.e., $r_k = 0.04$ and 0.40), respectively, and $F_L$ was 960 kN and 775 kN (i.e., $r_f = 0.61$ and 0.49), respectively. The BRB + RB and FD + RB peak force under retraction was −1700 kN at −63 mm deformation and −930 kN at −67 mm, respectively. The results from the experimental program show that design of full-scale deformable connections is feasible. Stable force-deformation response was achieved under full-scale seismic deformation demands. The BRB + RB has an order of magnitude lower $K_{el}$ than the FD + RB. The isotropic hardening of the BRB increases the initial yielding force. The wide spread availability of BRB is an advantage. The FD + RB has a reduced length limited-strength hysteretic component compared with the BRB + RB.

The experimental results were used to develop numerical models of the two deformable connections in OpenSEES [26]. The response of the calibrated numerical model of the BRB + RB connection is consistent with the experimental response, as seen by comparing the force-deformation behavior of the connection in Figure 15(a) and the time history of the hysteretic energy dissipation $E_h$ in Figure 15(b). The response of the calibrated numerical model of the FD + RB connection is consistent with the experimental response as shown in Figure 15(c) and (d).

Copyright © 2016 John Wiley & Sons, Ltd.

DOI: 10.1002/eqe

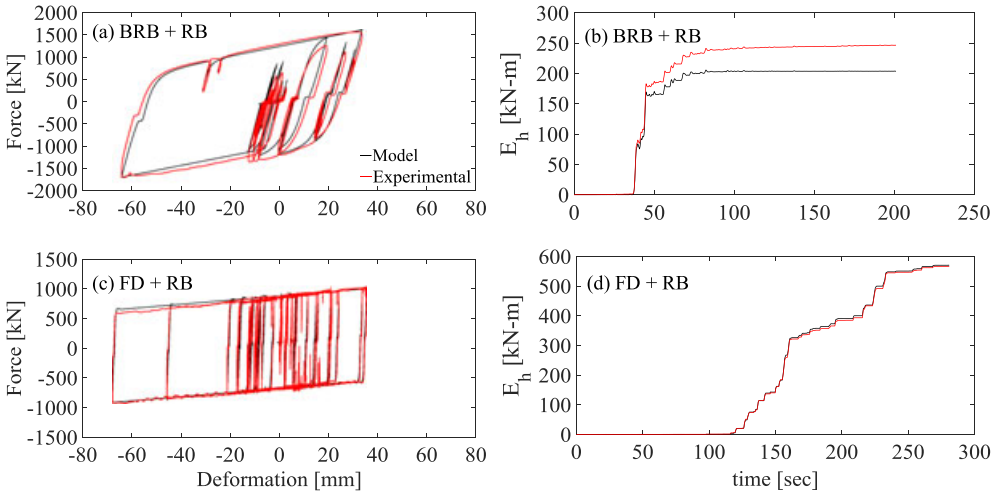



Figure 15. Calibrated numerical models for deformable connections compared with experimental results. RB, low damping laminated rubber bearings; BRB, buckling restrained brace; FD, friction device.

## 4. NUMERICAL EARTHQUAKE SIMULATIONS

Two sets of numerical simulations, denoted as NS1 and NS2, conducted using experimentally calibrated BRB + RB and FD + RB connections numerical models along with the baseline numerical model for the example building shown in Figure 2(a). Table IV lists the deformable connection parameters used in NS1 and NS2. $F_L$ in NS1 was similar to design case 1 (Table II). A larger $F_L$ was used in NS2, similar to design case 2 (Table II). Design concepts for the two deformable connection design cases where presented in Section 2.6. The 18 ground motions listed in Table I were used, and statistical results of the peak responses along the height of the structure are shown.

Figure 16(a) and (b) shows the 12th-floor BRB + RB and FD + RB force-deformation responses for EQ12 in NS1 and NS2, respectively. In NS1, the BRB isotropic hardening is mainly responsible for the smaller BRB + RB deformation demand compared with the FD + RB deformation demand. In NS2, the increased limiting strength $F_L$ reduces the deformation demand for both the BRB + RB and FD + RB connections compared with NS1.

Table V summarizes the maximum mean peak responses $\mu$ and standard deviation of these responses $\sigma$ from NS1 and NS2. $V_{LFRS}$, $F_c$, $\theta_{LFRS}$, $\theta_{GLRS}$, $D_c$, and $E_h$ denote the LFRS story shear, connection force, LFRS story drift, GLRS story drift, connection deformation, and connection hysteretic energy dissipation, respectively. The use of FD + RB connections reduces the maximum mean peak $V_{LFRS}$ by 54% and 45%, and the use of BRB + RB connections reduces the maximum mean peak $V_{LFRS}$ by 51% and 45% compared with the system with RE connections, in NS1 and NS2, respectively. The use of FD + RB connections reduces the maximum mean peak $F_c$ by 77% and 74%, and the use of BRB + RB connections reduces the maximum mean peak $F_c$ by 74% and 70% compared with the system with RE connections, in NS1 and NS2, respectively. The use of FD + RB connections reduces the maximum mean peak $\theta_{LFRS}$ by 41% and 13%, and the use of BRB + RB connections reduces the maximum mean peak $\theta_{LFRS}$ by 18% and 13%, in NS1 and NS2, respectively. The effect of the deformable connections on the maximum mean peak $\theta_{GLRS}$ appears to be small for both NS1 and NS2. The maximum mean peak $D_c$ and the maximum mean peak $E_h$ for the FD + RB connections in NS2 were 70% and 59% less, compared with NS1, respectively. The maximum mean peak $D_c$ and the maximum mean peak $E_h$ for the BRB + RB connections in NS2 were 38% and 19% less, compared with NS1, respectively. Thus, the use of deformable connections with a larger $F_L$ (in NS2) still leads to significant reductions in the maximum mean peak $F_c$ and maximum mean peak $V_{LFRS}$, similar to the reductions observed using deformable connections with a smaller $F_L$ (in NS1). The maximum mean peak $D_c$ was significantly reduced by increasing $F_L$.

Finally, the mean peak LFRS base hinge rotation for the system with the RE connections was 0.0052 rad. For the system with the FD + RB connections, it was decreased to 0.0012 and 0.0038 rad

Copyright © 2016 John Wiley & Sons, Ltd.

DOI: 10.1002/eqe

Table IV. Deformable connection parameters used in NS1 and NS2.

| | NS1 | | | NS2 | | |
|---|---|---|---|---|---|---|
| | $r_f$ | $r_k$ | $\alpha$ | $r_f$ | $r_k$ | $\alpha$ |
| BRB + RB | 0.610 | 0.044 | 0.057 | 0.910 | 0.060 | 0.053 |
| FD + RB | 0.490 | 0.400 | 0.005 | 0.980 | 0.400 | 0.005 |

BRB, buckling restrained braces; RB, low damping laminated rubber bearings; FD, friction device.

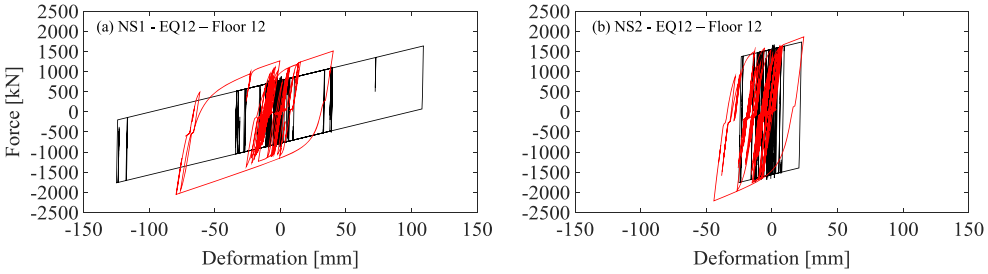



Figure 16. (a) NS1 and (b) NS2 12th-floor BRB + RB and FD + RB force-deformation due to EQ12.

Table V. Maximum mean peak ($\mu$) responses and their standard deviations ($\sigma$) from NS1 and NS2.

| | NS1 | | | | | | NS2 | | | | | |
|---|---|---|---|---|---|---|---|---|---|---|---|---|
| | $V_{LFRS}$ [kN] | $F_c$ [kN] | $\theta_{LFRS}$ [rad] | $\theta_{GLRS}$ [rad] | $D_c$ [mm] | $E_h$ [kNm] | $V_{LFRS}$ [kN] | $F_c$ [kN] | $\theta_{LFRS}$ [rad] | $\theta_{GLRS}$ [rad] | $D_c$ [mm] | $E_h$ [kNm] |
| $\mu^{RE}$ | 28156 | 7113 | 0.0110 | 0.0110 | 0 | 0 | 28156 | 7113 | 0.0110 | 0.0110 | 0 | 0 |
| $\mu^{FD+RB}$ | 12967 | 1654 | 0.0065 | 0.0116 | 111 | 1048 | 15495 | 1814 | 0.0096 | 0.0108 | 33 | 433 |
| $\mu^{BRB+RB}$ | 13683 | 1846 | 0.0090 | 0.0122 | 61 | 477 | 15541 | 2128 | 0.0096 | 0.0111 | 38 | 388 |
| $\sigma^{RE}$ | 10385 | 3485 | 0.0021 | 0.0021 | 0 | 0 | 10385 | 3485 | 0.0021 | 0.0021 | 0 | 0 |
| $\sigma^{FD+RB}$ | 985 | 157 | 0.0013 | 0.0019 | 20 | 679 | 1273 | 123 | 0.0019 | 0.0023 | 16 | 278 |
| $\sigma^{BRB+RB}$ | 913 | 181 | 0.0019 | 0.0020 | 14 | 264 | 1648 | 205 | 0.0020 | 0.0020 | 13 | 308 |

in NS1 and NS2, respectively. For the system with the BRB + RB connections, it was reduced to 0.0032 and 0.0040 rad in NS1 and NS2, respectively. Thus, increasing $F_L$ increased the rotation demand of the LFRS base hinge, but the increased rotation demand did not exceed the demand for the system with RE connections.

Figure 17 uses results from NS2 to show the deformable connection effect on the peak story/floor responses for each ground motion and the dispersion of the responses around the mean peak values, over the height of the structure.

Figure 17(a) shows that the peak $V_{LFRS}$ values for the systems with deformable connections are reduced in every story compared with the system with RE connections, and the peak $V_{LFRS}$ values are similar for the systems with BRB + RB and FD + RB connections. The dispersion of the peak $V_{LFRS}$ around the mean peak value is much smaller for the systems with deformable connections. Figure 17(b) shows the peak $F_c$ transferred from the floor systems to the LFRS. For the conventional system with RE connections, the largest mean peak $F_c$ values are at the 6th and 12th floors, and the smallest mean peak $F_c$ value is at the 10th floor. The use of the deformable connections successfully limits the peak $F_c$, the mean peak values of $F_c$ at each floor are similar, and the dispersion of the peak $F_c$ is significantly reduced. Figure 17(c) shows that the systems with BRB + RB and FD + RB connections have similar values of peak $\theta_{LFRS}$, which are smaller than those of the system with RE connections. Figure 17(d) shows that the three systems have similar peak $\theta_{GLRS}$ values. Figure 17(e) and (f) shows that the systems with BRB + RB and FD + RB connections

Copyright © 2016 John Wiley & Sons, Ltd.

DOI: 10.1002/eqe

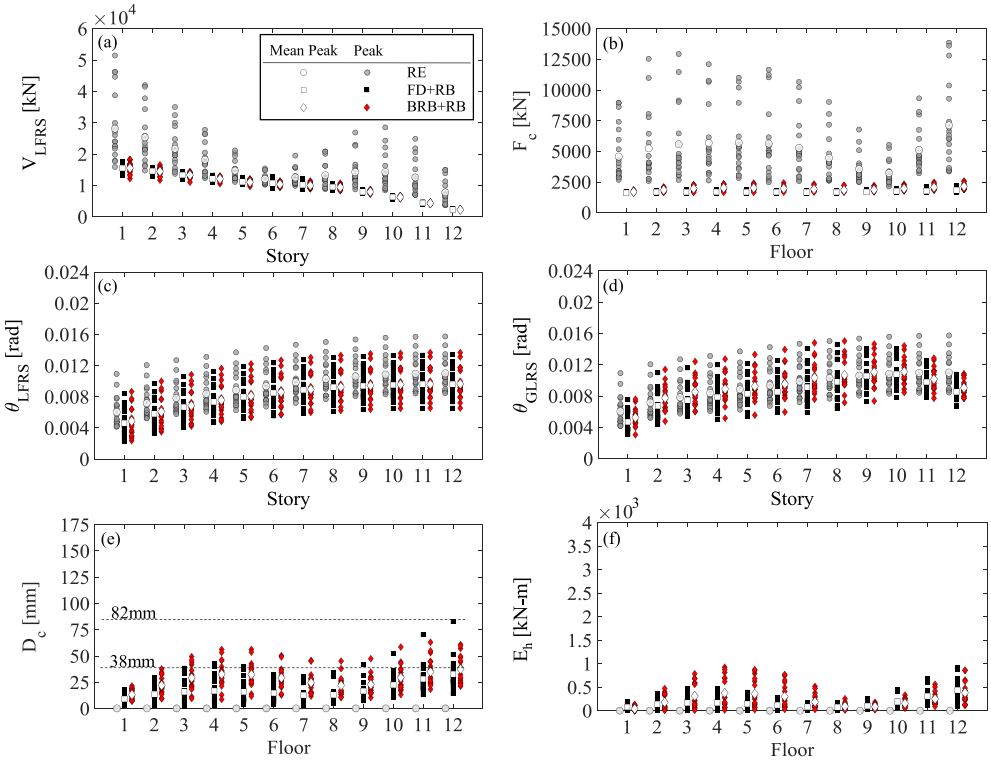



Figure 17. Peak and mean peak response quantities at each story/floor from NS2. RB, low damping laminated rubber bearings; BRB, buckling restrained brace; FD, friction device; RE, rigid elastic.

have similar peak $D_c$ and peak $E_h$ values. A small difference is observed in the lower floors where the BRB + RB connections have larger response.

Figure 18(a) shows the peak $a_f$ for the three systems. The pattern of the peak $a_f$ for the system with RE connections is similar to the pattern of the peak $F_c$ in Figure 17(b). The largest mean peak values of $a_f$ are at the 6th and 12th floors of the system with RE connections. At the 10th floor of the system with RE connections, the smallest mean peak $a_f$ is observed. These results are consistent with the results discussed in Section 2.2.3. The systems with the deformable connections have similar mean peak values of $a_f$, which are significantly smaller than those for the system with RE connections. These values are close to the mean peak ground acceleration $a_g = 0.54\,g$ shown in Figure 18(a) with a dashed line. The large dispersion of peak $a_f$ for the system with RE connections is reduced by using the deformable connections. The mean peak values of $a_f$ were averaged over the 12 floors of the building, and these results are 0.85, 0.46, and 0.51 g for the systems with RE, FD + RB, and BRB + RB connections, respectively.

Figure 18(b) shows the 5% damping pseudo acceleration response spectra for the 18 ground motions, the median pseudo acceleration spectrum, and the design response spectrum [25] for 5% damping. The design response spectrum value at the first mode period of the system with RE connections is 0.4 g. The dispersion of the ground motion spectral pseudo accelerations in the approximate period range of 0.1 to 0.6 s is large.

Figure 19(a)–(c) shows the mean floor pseudo acceleration response spectra for 5% damping calculated for $a_f$ at the 12th, 10th, and 6th floors, respectively. The periods of the three systems are given in Figure 19(b). The system with the RE connections has a significant 12th and 6th floor pseudo acceleration peak in the approximate period range of 0.1 to 0.6 s, where significant amplitude and dispersion of the ground motion spectral pseudo accelerations are observed in Figure 18(b). In the same range of periods, the 10th floor pseudo acceleration is not significant. The use of the BRB + RB or FD + RB connections reduces the 12th and 6th floor pseudo acceleration peaks from approximately 5 and 4 g, respectively, to approximately 2 g. The floor

Copyright © 2016 John Wiley & Sons, Ltd.

DOI: 10.1002/eqe

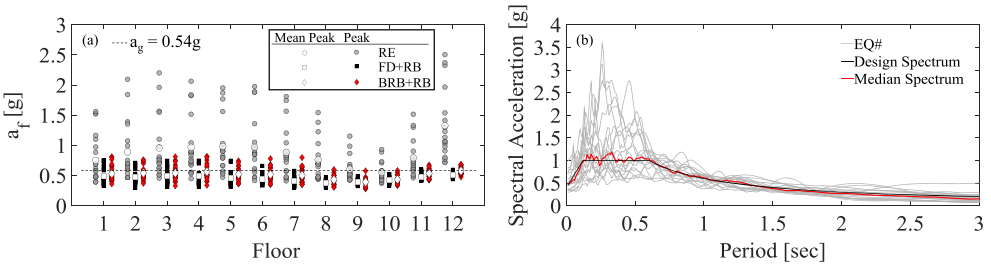



Figure 18. (a) Peak and mean peak floor total accelerations from NS2. (b) Pseudo acceleration response spectra for 18 ground motions, median pseudo acceleration spectrum, and design response spectrum [25] for 5% damping. RB, low damping laminated rubber bearings; BRB, buckling restrained brace; FD, friction device; RE, rigid elastic.

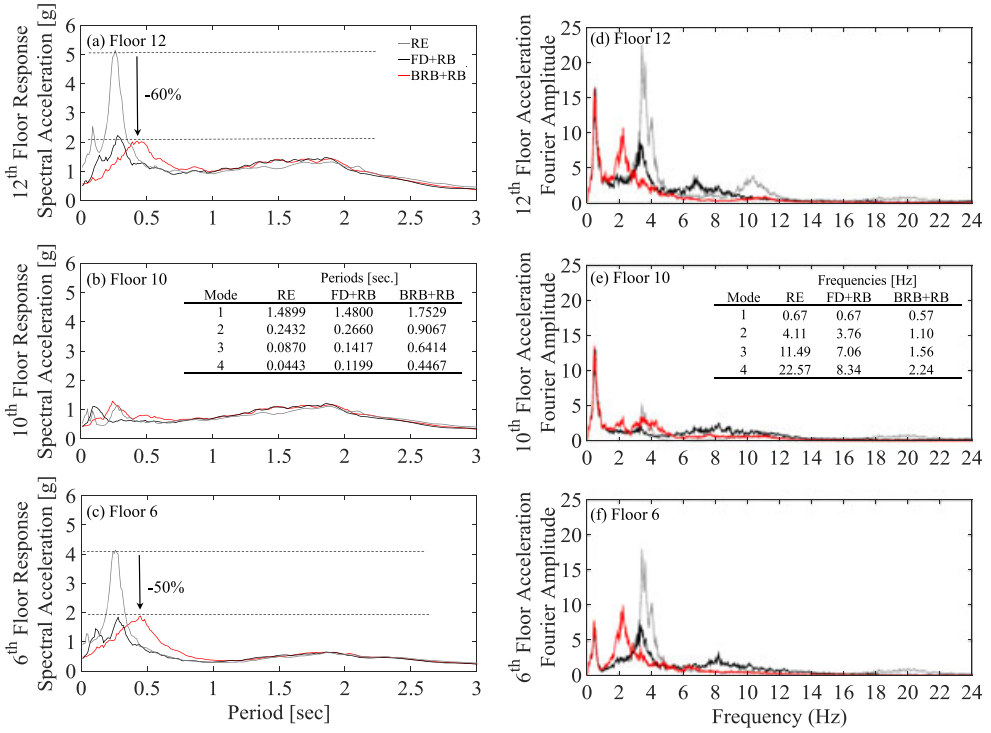



Figure 19. (a)–(c) Mean pseudo acceleration response spectra for floor total accelerations (5% damping) and (d)–(f) mean Fourier amplitude spectra for 12th, 10th, and 6th floor total accelerations respectively from NS2. RB, low damping laminated rubber bearings; BRB, buckling restrained brace; FD, friction device; RE, rigid elastic.

pseudo acceleration at longer periods is similar for the system with RE connections and the systems with deformable connections. Thus, the contributions of modes within the approximate period range of 0.1 to 0.6 s appear to be reduced by the deformable connections. At the 10th floor, near the node in the second mode shape, the floor pseudo accelerations for the three systems are similar.

The reduction in floor total acceleration response from modes within the approximate period range of 0.1 to 0.6 s from using the BRB + RB or FD + RB connections can be seen in the frequency domain, as well. Figure 19(d)–(f) show the mean Fourier amplitude spectra for the 12th, 10th, and 6th floor total accelerations, respectively. The frequencies of the first four modes are given in Figure 19(e). The system with RE connections has significant Fourier amplitude peaks for the 12th and 6th floor total accelerations in the approximate frequency range of 1.7 to 10.0 Hz (equivalent to the period range of 0.1 to 0.6 s). The use of deformable connections reduces the Fourier amplitude peaks within this

Copyright © 2016 John Wiley & Sons, Ltd.

DOI: 10.1002/eqe

approximate frequency range. For instance, at the 12th floor, the Fourier amplitude peak observed near 2.2 Hz of the system with BRB + RB connections, and the peak near 3.8 Hz of the system with FD + RB connections are much smaller than the peak near 4.1 Hz for the system with RE connections. Note that the system with BRB + RB connections has more closely spaced second, third, and fourth mode frequencies. The Fourier amplitude spectra for the 10th floor total acceleration are similar for the three systems.

## 5. SUMMARY

An initial parametric numerical study of an example building structure model with idealized deformable connection force-deformation responses was used to define feasible combinations of the limiting strength, elastic stiffness, and post-elastic stiffness of deformable connections used to connect the floor system to the LFRS of the building. BRB or FD were used as limited-strength hysteretic components, and RB were used as bearing components to provide out-of-plane stability of the LFRS. The responses of these two deformable connection configurations were evaluated experimentally at full scale. Numerical earthquake simulations of the example building model with calibrated BRB + RB and FD + RB deformable connections models were used to evaluate the response of the system with deformable connections in comparison with a system with conventional RE connections of the floor system to the LFRS.

## 6. CONCLUSIONS

1. The use of deformable connections between the floor system and the LFRS in an earthquake-resistant building system reduces the floor total accelerations, the LFRS story shears, and the forces transferred from the floor system to the LFRS compared with the results for a similar system with RE connections.
2. The use of deformable connections significantly reduces the dispersion of the floor total accelerations, the LFRS story shears, and the forces transferred from the floor system to the LFRS, so that more reliable design of earthquake-resistant building structures may be possible by using deformable connections.
3. Response spectra and Fourier amplitude spectra for the floor total accelerations show that higher-mode responses are reduced by using deformable connections compared with the results for a similar system with RE connections.
4. An approximate feasible design space was defined for the deformable connections for a 12-story reinforced concrete shear wall example building structure.
5. The design, construction, and installation of full-scale BRB + RB and FD + RB deformable connections were shown to be feasible.
6. The experimental responses of the deformable connections were shown to be stable under large deformations, and numerical models of the connections were developed to simulate the responses.
7. Numerical simulations show that the GLRS story drifts of systems with BRB + RB connections or FD + RB connections are similar to the drifts of a similar system with RE connections.
8. The use of BRB + RB connections or FD + RB connections led to reasonable connection deformations.

Studies of buildings with a different number of stories and with a LFRS other than a cantilever reinforced concrete shear wall may lead to different conclusions, and further studies are required.

ACKNOWLEDGEMENTS

This paper is based upon work supported by grants from National Science Foundation, award no. CMMI-1135033 in the George E. Brown, Jr. Network for Earthquake Engineering Simulation Research (NEESR) program and award no. CMMI-0402490 for the George E. Brown, Jr. Network for Earthquake Engineering

Copyright © 2016 John Wiley & Sons, Ltd.

DOI: 10.1002/eqe

Simulation (NEES) consortium operations. The authors are grateful for additional financial support provided by the Gerondelis Foundation, Yen Fellowship, and Lehigh University. The contributions of Zhi Zhang, Ulina Shakya, Arpit Nema, and the NEES@Lehigh and ATLSS Center staff are acknowledged. The authors appreciate the contributions of the companies DYMAT™, Star Seismic®, and Scan-Pac Mfg., Inc. Any opinions, findings, and conclusions expressed in this paper are those of the authors and do not necessarily reflect the views of the National Science Foundation or others acknowledged here.

## REFERENCES

1. Fleischman R, Farrow K. Dynamic behavior of perimeter lateral-system structures with flexible diaphragms. *Earthquake Engineering and Structural Dynamics* 2001; **30**(5):745–763.
2. Rodriguez M, Restrepo J, Carr A. Earthquake – induced floor horizontal accelerations in buildings. *Earthquake Engineering and Structural Dynamics* 2002; **31**:693–718.
3. Rodriguez M, Restrepo J, Blandon J. Seismic design forces for rigid floor diaphragms in precast concrete building structures. *Journal of Structural Engineering* 2007; **133**:1604–1615.
4. Kelly T. Floor response of yielding structures. *Bulletin of New Zealand National Society for Earthquake Engineering* 1978; **10**:255–272.
5. Ray-Chaudhuri S, Hutchinson T. Effect of nonlinearity of frame buildings on peak horizontal floor acceleration. *Journal of Earthquake Engineering* 2011; **15**:124–142.
6. Flores FX, Lopez-Garcia D, Charney FA. Assessment of floor accelerations in special steel moment frames. *Journal of Constructional Steel Research* 2015; **106**:154–165.
7. Sewell R, Cornell A, Toro G, McGuire R. A study of factors influencing floor response spectra in nonlinear multi-degree-of-freedom structures. The John A. Blume Earthquake Engineering Center Report No. 82, 1986.
8. Chopra AK. *Dynamics of Structures*. Pearson Prentice Hall: Berkeley,CA, California, 2007.
9. Roke D. Damage-free seismic-resistant self-centering concentrically-braced frames. Ph.D. Dissertation, Lehigh University, Bethlehem, PA, 2010.
10. Amaris Mesa AD. Dynamic amplification of seismic moments and shear forces in cantilever walls. M.Sc. Thesis, University of Pavia, Pavia, 2002.
11. Wiebe L, Christopoulos C. Mitigation of higher mode effects in base-rocking systems by using multiple rocking sections. *Journal of Earthquake Engineering* 2009; **13**:83–108.
12. Wiebe L, Christopoulos C, Trembley R, Leclere M. Mechanisms to limit higher mode effects in a controlled rocking steel frame. 1: concept, modelling, and low-amplitude shake table testing. *Earthquake Engineering and Structural Dynamics* 2013; **42**:1053–1068.
13. Skinner R, Kelly J, Heine A. Hysteretic dampers for earthquake resistant structures. *Earthquake Engineering and Structural Dynamics* 1975; **3**:287–296.
14. Key C. The seismic performance of energy absorbing dampers in building structures. *Bulletin of the New Zealand Society for Earthquake Engineering* 1984; **17**:38–46.
15. Luco JE, De Barros FCP. Control of the seismic response of a composite tall building modelled by two interconnected shear beams. *Earthquake Engineering and Structural Dynamics* 1998; **27**(3):205–223.
16. Mar D, Tipping S. *Smart Frame Story Isolation System: A New High-Performance Seismic Technology*. Tipping Mar and Associates: Berkeley, CA, 2000.
17. Amaris A, Pampanin S, Bull D, Carr A. Solutions to control and minimize floor damage in precast concrete buildings under severe earthquake loading, in *Proceedings NZ Concrete Industry Conference*, Rotorua, 2008.
18. Johnston H, Watson C, Pampanin S, Palermo A. Shake table testing of an integrated low damage building system, in *Second European Conference on Earthquake Engineering and Seismology*, Istanbul, 2014.
19. Robinson K. Advances in design requirements for buckling restrained braced frames, in *New Zealand Society of Earthquake Engineering Conference*, Auckland, NZ, 2014.
20. Crane ST. Influence of energy dissipation connections between floors and the lateral force resisting system, M.Sc. Thesis, University of California, San Diego, San Diego, CA, 2004.
21. Zhang D, Fleischman R, Restrepo J, Sause R, Maffei J, Mar D. Development of a floor inertial force limiting anchorage system building seismic response, in *10th National Conference on Earthquake Engineering*, Alaska, USA, 2014.
22. Fleischman R, Restrepo J, Nema A, Zhang D, Shakya U, Zhang Z, Sause R, Tsampras G, Monti G. Inertial force-limiting anchorage system for seismic resistant building structures, in 2015 *Structures Congress*, Portland, OR., 2015.
23. Tsamrpas G, Sause R, Fleischman RB, Restrepo JI. An earthquake-resistant building system to reduce floor accelerations, in *New Zealand Society for Earthquake Engineering Conference*, Rotorua, NZ, 2015.
24. G Tsampras, Sause R. Development and experimental validation of deformable connection for earthquake-resistant building systems with reduced floor accelerations, Network of Earthquake Engineering Simulation (NEES) Technical Report, 2015.
25. ASCE. *ASCE Standard ASCE/SEI7 – 10: Minimum Design Loads for Buildings and Other Structures*. American Society of Civil Engineers: Reston, Virginia, 2010.
26. McKenna F, Fenves GL, Scott MH, Jeremic B. Open system for earthquake engineering simulation (OpenSees), 2000. [Online]. Available: http://opensees.berkeley.edu/wiki/index.php/Main_Page. [Accessed 2014].

Copyright © 2016 John Wiley & Sons, Ltd.

DOI: 10.1002/eqe

27. FEMA P695. *Quantification of Building Seismic Performance Factors*. Federal Emergency Management: Washington, DC, 2009.
28. Baker JW. Conditional mean spectrum: tool for ground – motion selection. *Journal of Structural Engineering* 2011; **137**(3):322–331.
29. Whittaker A, Betrero V, Alonso J, Thompson C. Earthquake simulator testing of steel plate added damping and stiffness elements, Earthquake Engineering Research Center Report UBC/EERC-89/02, 1989.
30. Tsai K-C, Chen H-W, Hong C-P, Su Y-F. Design of steel triangular plate energy absorbers for seismic-resistant construction. *Earthquake Spectra* 1993; **9**(3):505–528.
31. Tsai CS, Tsai KC. TPEA device as seismic damper for high-rise buildings. *Journal of Engineering Mechanics* 1995; **121**(10):1075–1081.
32. Dargush GF, Soong TT. Behavior of metallic plate dampers in seismic passive energy dissipation systems. *Earthquake Spectra* 1995; **11**(4):545–568.
33. Black CJ, Makris N, Aiken ID. Component testing, seismic evaluation and characterization of buckling-restrained braces. *Journal of Structural Engineering* 2004; **130**(6):880–894.
34. Fahnestock LA, Sause R, Ricles JM. Seismic response and performance of buckling-restrained braced frames. *Journal of Structural Engineering* 2007; **133**(9):1195–1204.
35. Merritt S, Uang C-M, Benzoni G. Subassemblage testing of Corebrace buckling restrained braces, Report No. TR-2003/01, University of California, San Diego, San Diego, 2003.
36. Pall AS. Limited slip bolted joints – a device to control seismic response of large panel structures, Ph.D. Dissertation, Concordia University, Montreal, Quebec, Canada, 1979.
37. FitzGerald TF, Anagnos T, Goodson M, Zsutty T. Slotted bolted connections in aseismic design for concentrically braced connections. *Earthquake Spectra* 1989; **5**(2):383–391.
38. Grigorian CE, Yang TS, Popov EP. Slotted bolted connection energy dissipators. *Earthquake Spectra* 1993; **9**(3):491–504.
39. Chi B, Uang C-M. Dynamic testing of full-scale slotted bolted connections, Report No. TR-99/05, Department of Structural Engineering, University of California, San Diego, 2000.
40. Wolski M, Ricles JM, Sause R. Experimental study of a self-centering beam–column connection with bottom flange friction device. *Journal of Structural Engineering* 2009; **135**(5):479–488.
41. Lin Y-C, Sause R, Ricles J. Seismic performance of a large-scale steel self-centering moment-resisting frame: MCE hybrid simulations and quasi-static pushover tests. *Journal of Structural Engineering* 2013; **139**(7):1227–1236.
42. Robinson WH, Greenbank LR. Properties of an extrusion energy absorber. *Bulletin of the New Zealand National Society for Earthquake Engineering* 1975; **8**(3):187–191.
43. Cousins WJ, Porritt TE. Improvements to lead – extrusion damper technology. *Bulletin of the New Zealand National Society for Earthquake Engineering* 1993; **26**(3):342–348.
44. Christopoulos C, Trembley R, Kim HJLM. Self-centering energy dissipative bracing system for the seismic resistance of structures: development and validation. *Journal of Structural Engineering* 2008; **134**(1):96–107.
45. Chou C-C, Chung P-T. Development of cross-anchored dual-core self-centering braces for seismic resistance. *Journal of Constructional Steel Research* 2014; **101**:19–32.
46. Chou C-C, Chung P-T. Development of steel dual-core self-centering braces: quasi-static, cyclic tests, and finite element analyses. *Earthquake Spectra* 2015; **31**:247–272.
47. Chou C-C, Wu T-H, Beato ARO, Chung P-T, Chen Y-C. Seismic design and tests of a full-scale one-story one-bay steel frame with a dual-core self-centering brace. *Engineering Structures* 2016; **111**:435–450.
48. Miller DJ, Fahnestock LA, Eatherton MR, Self-centering buckling-restrained braces for advanced seismic performance, in *Structures Congress*, Las Vegas, NV, 2011.
49. Nims DK, Richter PJ, Bachman RE. The use of the energy dissipating restraint for seismic hazard mitigation. *Earthquake Spectra* 1993; **9**(3):467–489.
50. Inaudi JA, Nims DK, Kelly JM. On the analysis of structures with energy dissipating restraints. Earthquake Engineering Research Center Report UBC/EERC-93/13, Berkeley, CA, 1993.
51. Piedrafita D, Cahis X, Simon E, Comas J. A new modular buckling restrained brace for seismic resistant buildings. *Engineering Structures* 2013; **56**:1967–1975.
52. Piedrafita D, Maimí P, Cahis X. A constitutive model for a novel modular all-steel buckling restrained brace. *Engineering Structures* 2015; **100**:326–331.
53. Huang YN, Whittaker AS, Luco N. Seismic performance assessment of base-isolated safety-related nuclear structures. *Earthquake Engineering and Structural Dynamics* 2010; **39**:1421–1442.
54. Constantinou M, Whittaker A, Kalpakidis Y, Fenz D, Warn G. Performance of seismic isolation hardware under service and limit loading. State of California Department of Transportation Project, 2007.
55. Naeim F, Kelly JM. *Design of Seismic Isolated Structures: From Theory to Practice*. John Wiley & Sons, Inc.: New York, USA 1999.
56. Kelly JM, Takhirov SM. Analytical and experimental study of fiber-reinforced elastomeric isolators. PEER 2001/11, Berkeley, CA, 2001.
57. Huang Y-N, Whittaker AS, Luco N. Seismic performance assessment of base-isolated safety-related nuclear structures. *Earthquake Engineering and Structural Dynamics* 2010; **39**:1421–1442.
58. AASHTO. *LRFD Bridge Design Specification*. American Association of State Highway and Transportation Officials: Washington, DC, 2010.

Copyright © 2016 John Wiley & Sons, Ltd.

DOI: 10.1002/eqe

59. AASHTO. Guide specifications for seismic isolation design, 2010.
60. Kelly J, Konstantinidis D. *Mechanics of Rubber Bearings for Seismic and Vibration Isolation*. John Wiley and Sons Ltd.: West Sussex, United Kingdom 2011.
61. Lindley P. Engineering design with natural rubber, NR Technical Bulletins. The Malaysian Rubber Producers' Research Association, 1978.

Copyright © 2016 John Wiley & Sons, Ltd.

DOI: 10.1002/eqe